



Tetrathiafulvalenes as anchors for building highly conductive and mechanically tunable molecular junctions

Qi Zhou^{1,2,3}, Kai Song^{1,3}, Guanxin Zhang^{1,2} , Xuwei Song^{1,2}, Junfeng Lin^{1,2}, Yaping Zang^{1,2} ,
Deqing Zhang^{1,2} & Daoben Zhu¹

The interface between molecules and electrodes has great impact on charge transport of molecular devices. Precisely manipulating the structure and electronic coupling of electrode-molecule interface at a molecular level is very challenging. Here, we develop new molecular junctions based on tetrathiafulvalene (TTF)-fused naphthalene diimide (NDI) molecules which are anchored to gold electrodes through direct TTF-Au contacts formed via Au-S bonding. These contacts enable highly efficient orbital hybridization of gold electrodes and the conducting π -channels, yielding strong electrode-molecule coupling and remarkably high conductivity in the junctions. By further introducing additional thiohexyl (SHe) anchors to the TTF units, we develop molecular wires with multiple binding sites and demonstrate reversibly switchable electrode-molecule contacts and junction conductance through mechanical control. These findings show a superb electrode-molecule interface and provide a new strategy for precisely tuning the conductance of molecular devices towards new functions.

¹Beijing National Laboratory for Molecular Sciences, CAS Key Laboratory of Organic Solids, Institute of Chemistry, Chinese Academy of Sciences, 100190 Beijing, China. ²University of Chinese Academy of Sciences, 100049 Beijing, China. ³These authors contributed equally: Qi Zhou, Kai Song.
✉email: gxzhang@iccas.ac.cn; zangyaping@iccas.ac.cn

Charge transport across electrode-molecule interface plays significant roles in determining the properties and functions of molecular electronic devices^{1–4}. Typically, terminal anchors are introduced to molecular bridges to form electrode-molecule contacts and modify the interfacial interactions and structures^{5–7}. For instance, amines⁸, thioethers^{9,10}, and pyridines¹¹ are commonly used as anchors to bind to gold electrodes through dative interactions, while thiol¹² and alkyne¹³ anchors have been used to form covalent gold-sulfur (Au-S) and gold-carbon (Au-C) contacts. It is worth noting that, besides the nature of the electrode-molecule contacts, the orbital overlap between anchors and molecular bridges is also a key factor in determining the interfacial electronic coupling strength. In general, a metal-anchor bond that aligns with conjugated orbitals of molecular bridges can provide efficient interfacial orbital mixing and facilitates charge transport. However, it is challenging to precisely control the electrode-molecule contact geometry in molecular devices, and the misalignment between the metal-anchor bond and the conducting channel introduces additional resistance that lowers the conductance of the device.

Tetrathiafulvalene (TTF) finds important applications in organic conducting materials^{14–16}, supramolecular chemistry^{17,18}, and molecular machines^{19,20} due to its remarkable electron-donating ability and redox properties. TTF is also regarded as an important unit in molecular electronics since it was proposed as a building unit of the first theoretical model of the single molecular rectifier in 1974^{21–24}. Since then, several TTF or π -extended tetrathiafulvalene (exTTF)-based molecular wires have been prepared by incorporating TTF or exTTF active center into the molecular backbone. In these systems, additional terminal anchors (thiol or thioether) are required to connect the TTF or exTTF molecular bridge to the electrode^{25–28}. Using these anchors, however, increases the length and flexibility of the molecules, hence leading to a lower conductance. Herein, we report new TTF-fused naphthalene diimide molecular wires that can bind to gold electrodes and form single-molecule junctions through direct TTF-Au coupling in which the sulfur atoms of TTF bind to gold electrodes to form the Au-S bonds. In these junctions, the Au-S bonds are nearly coplanar with conjugated molecular orbitals. This produces strong electronic coupling at the electrode-molecule interface, which further leads to remarkable high conductance of $10^{-2} G_0$ over a transport length of ~ 1.5 nm. We further introduce additional thiohexyl anchors to the terminal TTF units by taking advantage of their chemical modification feasibility. We show that the electrode-molecule binding sites in these wires can be either TTF-Au or thiohexyl-Au modes (see below), and importantly these binding sites can be mechanically controlled in a reversible manner, yielding tunable interfacial electronic coupling and hence the conductance of the single-molecule devices. These findings demonstrate that TTF can act as both functional unit and anchor for constructing highly conducting molecular wires, and offering a new way of modulating interfacial properties of molecular devices through mechanical control.

Results

Synthesis of NDITTF molecules. We design and synthesize TTF-based molecular wires NDITTF-MF and NDITTF-SHe (see Fig. 1) according to the procedures detailed in the Supplementary information (Supplementary Fig. 1)²⁹. These wires contain an electron acceptor naphthalene diimide (NDI) core, which is flanked with two TTF units and forms a conjugated electron donor-acceptor-donor (D-A-D) framework. Various terminal substituents are incorporated into TTF units to modulate the interaction between molecules with gold electrodes. Long alkyl side chains are introduced to improve their solubilities in organic solvents. The unique D-A-D structure facilitates electron delocalization across the molecular backbone and produces long

wave-length absorptions and small HOMO-LUMO gaps, as demonstrated by ultraviolet-visible (UV-vis) absorption spectroscopy and cyclic voltammetry (CV) characterizations (Supplementary Figs. 2 and 3).

We repeat the STM-BJ measurements for thousands of times and compile the conductance traces into one-dimensional (1D) log-binned histograms and two-dimensional (2D) conductance-displacement histograms without any data selection. Histograms for measurements at different biases are shown in Fig. 2 and Supplementary Fig. 4. The 1D histograms show peaks around integer multiples of G_0 due to the formation of point gold contacts, and a bias-independent high conductance peak at $\sim 10^{-2} G_0$ corresponding to molecular junctions. Although NDITTF molecules are redox active (as shown in the CV curves in Supplementary Fig. 3), a redox process unlikely happens during the STM-BJ measurements, since an electrochemical redox reaction usually leads to a noticeable conductance shift with bias^{31,32}. Further, the 2D histogram shows that the extension length of the molecular conductance plateau is ~ 1 nm. This indicates that the single-molecule junctions are formed across a molecule of ~ 1.5 nm by accounting for the ~ 0.5 nm Au relaxation gap upon rupture of Au contacts³³.

To further explore the electrode-molecule interactions in these junctions, we measure the NDI based control molecule **1** in a similar environment. As can be seen from Supplementary Fig. 5, there is no well-defined molecular conductance features, thereby ruling out a possible NDI-Au-binding mechanism. Since it is known that carboxylic acid methyl ester group typically does not bind to gold electrode, we hypothesize that the junctions are formed through the interactions between TTF and Au electrodes. Note that TTF itself does not yield clear molecular conductance features (see Supplementary Fig. 6), suggesting that the junctions are formed across the NDI backbone driven by TTF-Au interactions at the two sides of the molecules.

Theoretical analysis. To understand the properties of single-NDITTF-MF junctions, we first perform density functional theory (DFT)-based calculations to examine its optimized molecular geometry and orbitals. Figure 2c shows the frontier orbitals HOMO and LUMO, which are most relevant to the transport in molecular devices. We see that both HOMO and LUMO are delocalized across the entire D-A-D molecular backbone. It should be noted that TTF is not aromatic, which is reflected by the boat-shaped conformation of TTF unit³⁴. The orbital overlap between the S lone pairs and gold electrodes enables the formation of σ donor-acceptor S-Au bond aligned with the conducting π channel. The partial charge transfer from TTF to Au at the molecule-electrode interface promotes the transition of TTF towards a more aromatic form, producing an aromatic stabilization effect^{35–39}. Contrary to other thioether anchors^{9,10}, such aromatic stabilization effect provides the additional driving force for forming stable S-Au contacts. This unique effect presented in TTF not only leads to a relatively strong contact between molecule and electrode but also enables a direct orbital hybridization between Au and the delocalized conducting π -channels of the entire NDITTF backbone, yielding a strong interfacial electronic coupling and high conductance.

We next turn to DFT calculations to better understand their conducting properties using the FHI-Aims package with a Perdew-Burke-Ernzerhof (PBE) exchange-correlation functional^{40–42}. The calculation details are shown in the Supplementary information. In each of the TTF unit, there are four S atoms that can in principle bind to gold electrodes. However, the outer S atoms show stronger binding abilities than the inner ones, due to the electron withdrawing effect caused by the NDI unit. Specifically, the inner S $p\pi$ orbitals can

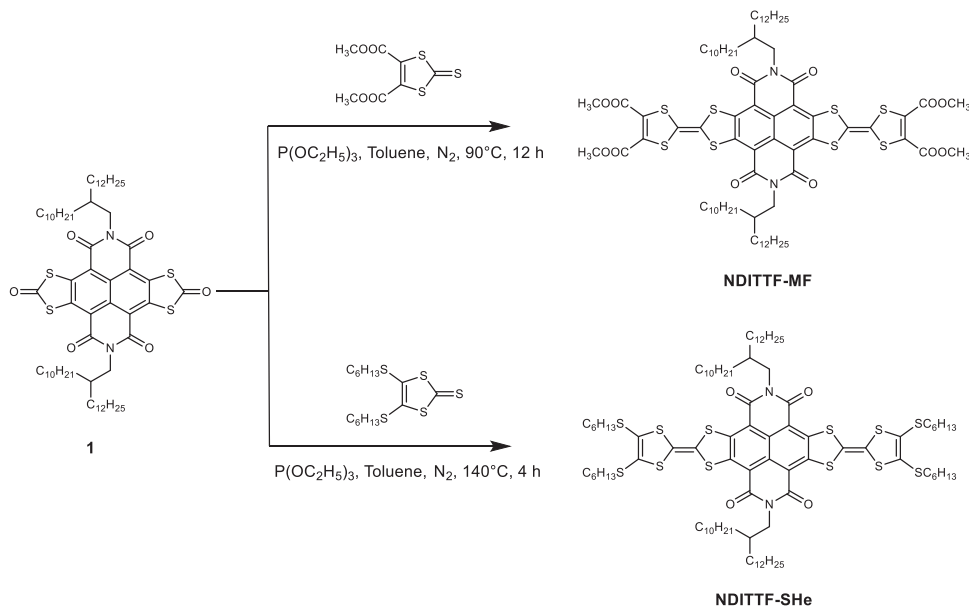


Fig. 1 Chemical structures of NDITTF-MF and NDITTF-SHe and their synthetic approaches. Conductance measurements. We firstly probe the electronic transport properties of the four carboxylic acid methyl ester groups terminated TTF molecule (NDITTF-MF, see Fig. 1) using the scanning tunneling microscope-break junction (STM-BJ) technique (Fig. 2a), which can measure single-molecule conductance at room temperature in ambient environment^{8,30}. Briefly, we repeatedly drive a gold STM tip in and out of contact with a gold substrate in 1,2,4-trichlorobenzene (TCB) solution of NDITTF-MF molecule (0.01–0.1 mM). After the Au–Au point contact is broken, the molecule can bridge the two electrodes and form a single-molecule junction. We measure the conductance as a function of the tip–substrate displacement during this process. The inset of Fig. 2b shows sample conductance traces of NDITTF-MF measured at an applied tip bias of 0.5 V. A clear conductance plateau appears at $\sim 10^{-2} G_0$ (where $G_0 = 2e^2/h$ is the quantum of conductance), indicating the formation of single-molecule junctions of NDITTF-MF.

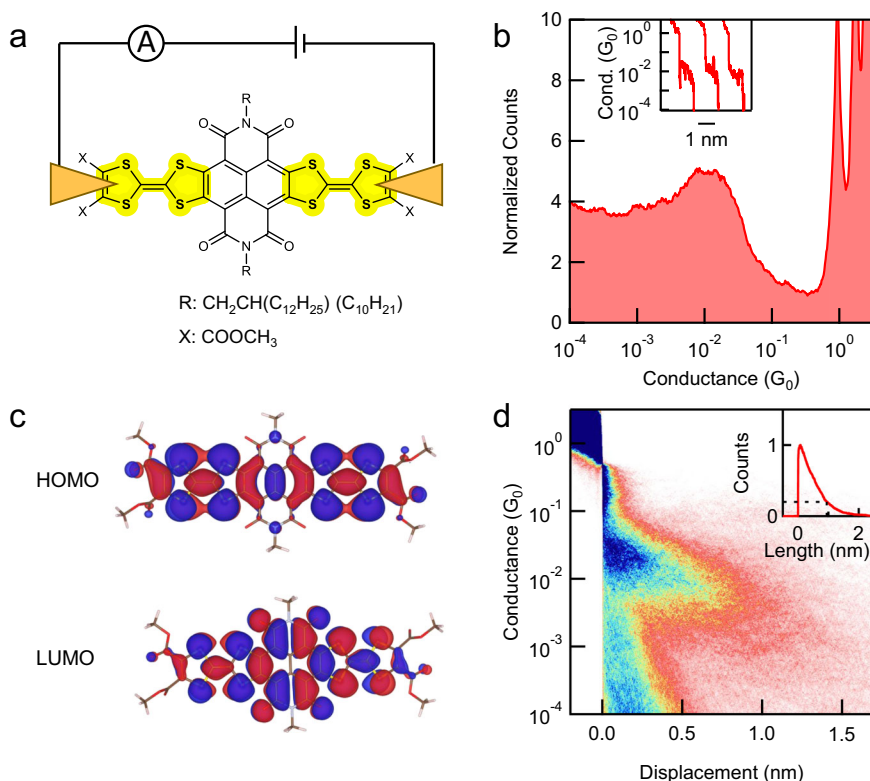


Fig. 2 STM-BJ measurement results of NDITTF-MF. **a** Schematic of a single-NDITTF-MF molecule junction. **b** Logarithm-binned 1D histograms for NDITTF-MF measured at an applied bias voltage of 0.5 V. Inset: Sample conductance traces. **c** Gas-phase HOMO and LUMO orbitals of NDITTF-MF. **d** 2D conductance-displacement histograms for NDITTF-MF. Inset: Normalized length profiles determined from the 2D histogram. All histograms are compiled from 10,000 traces without data selection.

delocalize with the NDI core, whereas the outer ones are more localized, enabling them to form stronger dative contacts with the electrode. To identify the Au–S binding configurations, we model various Au–S binding modes and calculated their binding energies. As shown in Supplementary Fig. 7, the binding energy for the outer Au–S binding mode (0.56 eV) is higher than that of the inner Au–S (0.45 eV) and the Au–2S (one inner S atom and one outer S atom, 0.28 eV) bindings, suggesting that the outer Au–S binding is dominant. There might exist more complicated binding modes through multiple Au atoms and S atoms in single TTF. However, it is not straightforward to build a suitable model to simulate such bindings due to the incompatible geometries between the TTF unit and the available Au cluster models. Nevertheless, the outer Au–S binding should be the dominant scenario since this configuration (see Supplementary Fig. 8) is more in line with the measured junction length (~ 1.5 nm).

We then perform transport calculations of single-NDITTF-MF junctions. Figure 3a shows two sample junctions formed by connecting Au to the outer S atoms of TTF in a *cis* and *trans* conformation. We see that Au–S bonds are nearly perpendicular to the molecular backbone in the optimized junction geometry. This contact geometry enables the mixing of the orbitals of gold and the delocalized molecular π -orbitals, facilitating charge transport across the single-molecule junctions. Figure 3b shows that the calculated transmission spectra are almost identical for the two types of junctions. We emphasize that strong coupling between electrodes and molecular orbitals exist, as reflected by the significant peak spread of HOMO and LUMO resonances. Such strong coupling leads to remarkably high transmission probabilities ($\sim 0.5 G_0$) at the Fermi energy (E_F). The isosurface plots of the transmitting eigenstate at E_F show a strong hybridization between gold and the delocalized molecular orbitals (see the inset of Fig. 3b), thus explaining the large interfacial coupling and high transmission probability. These calculations rationalize the observed high conductance of single-NDITTF-MF junctions at a low bias where the transport is dominated by a typical off-resonant transport mechanism.

Conductance comparisons. We find that the peak conductance (1D histogram) of the NDITTF-MF molecule obtained at off-resonant transport regime is much higher than that of other conjugated molecular wires with similar length (Table 1). Further, we note that the molecular conductance plateau shown in the 2D histogram (Fig. 2d) is slightly sloped. This feature might be caused by the change of Au–S binding sites, or variations of molecular geometries or electrode–molecule interactions occurred during junction elongation^{43,44}. We emphasize that, even though

we measure the conductance near the end of the conductance plateau (see the details in the Supplementary Fig. 9), the conductance of NDITTF ($10^{-2.2} G_0$) is still higher than most of the molecular wires shown in Table 1. These findings demonstrate that NDITTF-MF is a new core for building highly conductive molecular wires.

Charge transport of thiohexyl modified NDITTF. It is known that TTF moiety can be easily substituted or modified with simple synthetic procedures¹⁴. By taking advantage of this feature, we design and synthesize a new TTF derivative (NDITTF-SHe, Fig. 4a) by replacing terminal carboxylic acid methyl ester groups by thiohexyls, which are common anchors used for forming dative Au–S contacts with gold electrodes (see Supplementary Information for the synthetic details). We then measured its single-molecule conductance in a similar environment using STM-BJ techniques. The 1D histograms reveal two distinct molecular conductance peaks located at $\sim 10^{-2} G_0$ (High_G) and $\sim 5 \times 10^{-4} G_0$ (Low_G) (Fig. 4b). Figure 4c shows the corresponding 2D histograms containing two molecular conductance plateaus with different lengths. We note that the conductance values and plateau lengths of the High_G feature are in good agreement with those of the single-NDITTF-MF junctions (Supplementary Figs. 10 and 11), suggesting a similar junction structure defined by the direct TTF–Au coupling. By contrast, the Low_G conductance plateau extends much longer (~ 1.9 nm), indicating a longer conducting pathway across the two electrodes. We hence hypothesize that a new type of single-molecule junctions is formed through dative Au–S bonding in terminal thiohexyls.

To gain more insight of the transport properties, we calculate the molecular orbitals and transmission functions of single-NDITTF-SHe junctions with different binding scenarios (Fig. 4c and Supplementary Figs. 12–13). We first note from the HOMO and LUMO orbitals that the electron delocalization is across the NDITTF core, in agreement with that in NDITTF-MF. The calculated transmission functions are shown in Fig. 4d. We see that the junction formed through dative bonds between Au and S atoms in TTF units yields strong orbital couplings and a high transmission level at E_F . This is consistent with what has been observed for the single-NDITTF-MF junctions. By contrast, much weaker couplings as reflected by the narrower resonance peaks are observed when forming junctions through terminal SHe–Au bonding. The decreased electrode–molecule coupling is attributed to the weakened orbital mixing of gold electrodes and the π orbital of the molecular backbone, which is always observed for molecular wires terminated with the similar thioether anchors⁵⁴, and leads to a lower transmission at E_F . This hence accounts for the measured lower conductance. It should be further noticed that the existence of two different conductance states

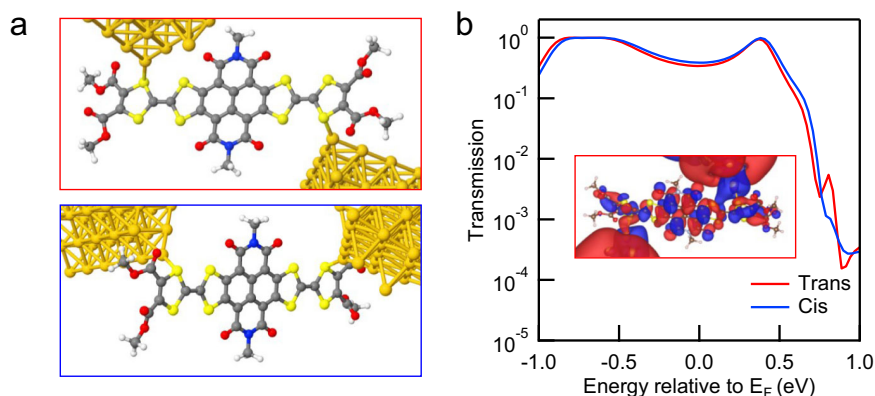
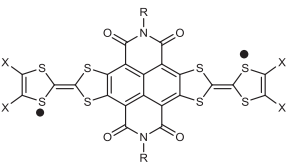
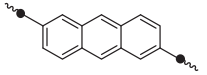
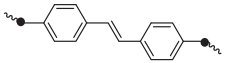
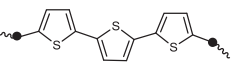
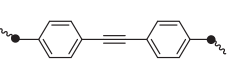
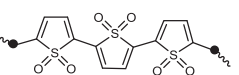
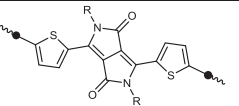
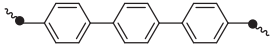
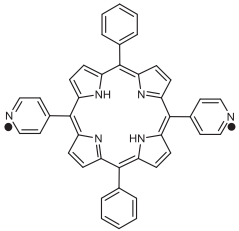
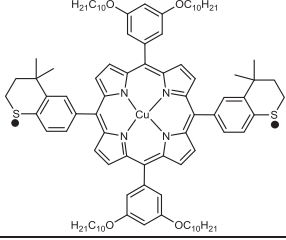


Fig. 3 DFT-based transmission calculations of NDITTF-MF. **a** Junction structures used to compute the junction transmission functions. **b** Transmission functions against energy of the two types of junctions. Inset: Eigenstate at the Fermi energy for the junction in a *trans* conformation.

Table 1 Comparison of the reported and proposed molecular wires^{45–53}.

Molecule	Structure	Conductance (Log G/G_0)	Length (nm)	References
NDITTF-MF		−1.98	1.48	This work
Anthracene		−2.85	1.03	45
Oligo-(phenylene vinylene) OPV		−2.92	1.23	46
Oligo-thiophene		−3.30	1.23	47
Oligo-(phenylene ethynylene) OPE		−2.11	1.25	48
Oligo-(thiophene-1,1-dioxide) TDO		−3.80	1.30	49
Diketopyrrolopyrrole DPP		−3.00	1.34	50
Terphenyl		−3.35	1.42	51
Diphenylporphyrin (p-DPP)		−3.59	1.55	52
Copper-containing Porphyrin		−4.46	1.80	53

The molecular length is defined by the distance between black dots on the two sides of the molecules.

in single-NDITTF-SHe junctions suggest that their conducting properties can be modulated through altering the electrode-molecule binding sites and hence the interfacial electronic coupling.

Mechanically controlled switching measurements. Given the unique structure and conducting properties of the NDITTF-SHe, we turn to modified STM-BJ measurements to explore the

mechanical tunability of the electrode-molecule coupling within individual single-NDITTF-SHe junctions (Fig. 5a). To do so, we first form a single-molecule junction, and then modulate the tip-substrate separation with an amplitude of 0.3 nm for three cycles before rupturing the junction (Fig. 5b). We obtain the 2D conductance-time histograms by aligning traces that start at a conductance corresponding to the Low_G peak shown in Fig. 4a (see Supplementary Fig. 14 for the details of data analysis). We

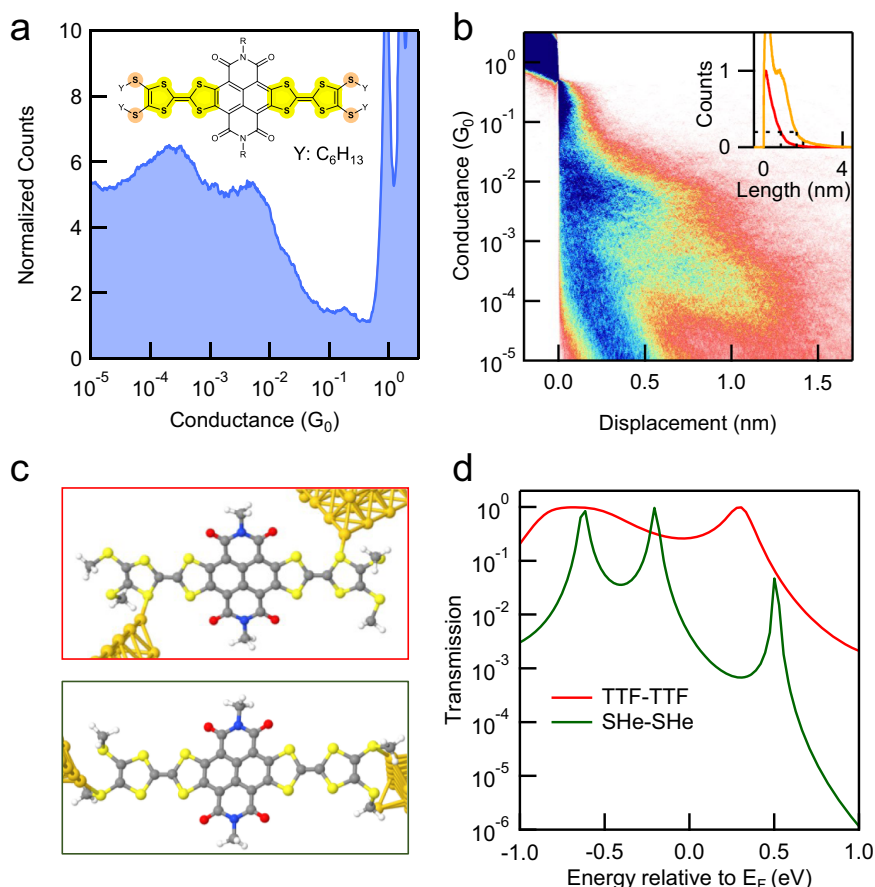


Fig. 4 Charge transport properties of NDITTF-SHe. **a** Logarithm-binned 1D histograms for NDITTF-SHe at an applied bias of 0.5 V. Inset: Molecular structure of NDITTF-SHe. **b** 2D conductance-displacement histograms for NDITTF-SHe at an applied bias of 0.5 V. All histograms are compiled from 10,000 traces without data selection. Inset: Normalized length profiles determined from the 2D histogram. **c** Junction structures with different binding sites used to compute the junction transmission functions. **d** Transmission functions against energy of the two types of junctions.

see that the conductance reversibly switches between the Low_G and High_G states during the elongation and compression of the junctions, which is evidenced by the conductance profiles shown in Fig. 5c. We also perform the switching measurements with a piezo ramp of 0.5 nm and observe very similar conductance switching characteristics (Supplementary Fig. 15). This indicates that the switching between the Low_G and High_G state is not sensitive to the piezo ramp length, and these two conductance states are stable. Note that the binding energies of S in different positions to Au electrodes are nearly identical (0.6–0.7 eV, as shown in Supplementary Tables 1 and 2). These results thus suggest that the electrode-molecule linkages are mechanically reorganized by shifting the binding sites between the SHe and TTF S atoms (Fig. 5a), yielding the mechanical switch of interfacial electronic coupling strength and the junction conductance. Since there could be three main binding configurations, namely TTF-TTF, TTF-SHe, and SHe-SHe, one might expect three different conductance states. However, as suggested by DFT calculations (Supplementary Fig. 16), the conductance of the SHe-SHe and TTF-SHe configurations are very similar. This explains the observation that only two conductance states are present in the switching measurement.

To further validate this binding site switching mechanism, we perform similar measurements for the control molecule NDITTF-MF without SHe anchors. The results shown in Supplementary Fig. 15 suggest that this molecule only has minor conductance change compared with that of the NDITTF-SHe molecule, hence supporting the proposed switching mechanism. We emphasize that,

the applied piezo ramp may not directly correspond to the length difference defined by different binding sites, since the molecular orientation might not be perfectly aligned with the tip-substrate direction. Additionally, the orientation of the molecule might change during the piezo ramp. Previously, several mechanically controlled switches have been demonstrated in molecular systems with multiple binding sites^{3,55–57}. Our findings reported here provide a new design for mechanical molecular switches building on strongly coupled systems.

Discussion

In conclusion, we demonstrate TTF to be a unique anchor that can offer strong electrode-molecule electronic coupling which is further translated into remarkably high conductance of single-molecule junctions. By introducing additional thiohexyl anchors to the TTF unit, we develop molecular wires with multiple binding sites and achieve mechanically tunable conductivity through reversibly changing the Au-S binding sites as well as interfacial couplings. This work offers new strategies to precisely modulate the electrode-molecule coupling character and sheds light for designing new functional interfaces and molecular devices.

Methods

STM-BJ measurements. Single-molecule conductance measurements were performed in ambient conditions and room temperature using a custom-built scanning tunneling microscope-break junction (STM-BJ) setup. During the STM-BJ measurements, we repeatedly drive a gold STM tip in and out of contact with a gold substrate in 1,2,4-trichlorobenzene (TCB) solution of NDITTF molecules

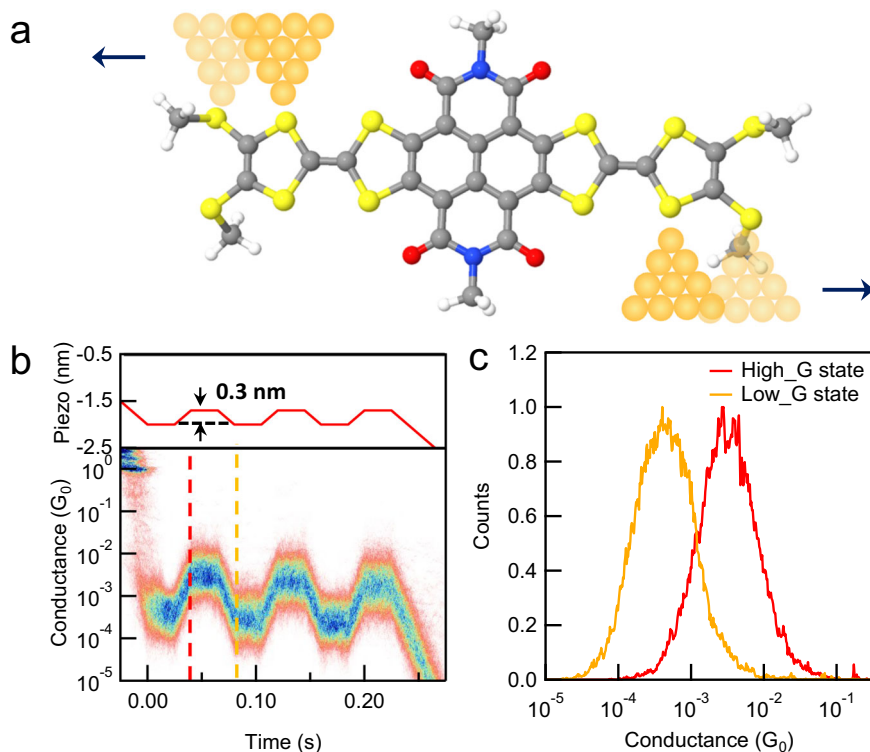


Fig. 5 Mechanically controlled switching measurements. **a** Schematics of the single-NDITTF-SHE molecule junctions formed during the STM tip-substrate displacement modulation. **b** Piezo displacement as a function of time (top) and 2D conductance-time histograms obtained during displacement modulations. The 2D histogram is constructed from 733 traces selected out of total 20,000 traces. **c** Line profiles comparing the conductance in different regions.

(0.01–0.1 mM). After the Au–Au point contact is broken, the molecule can bridge the two electrodes and form a single-molecule junction. We measure the conductance as a function of the tip-substrate displacement during this process. One-dimensional conductance histograms and the two-dimensional conductance histograms were constructed by compiling thousands of collected conductance traces.

DFT-based calculations. We carried out density functional theory (DFT) calculations using the Perdew–Burke–Ernzerhof (PBE) exchange–correlation functional implemented by the Fritz Haber Institute ab initio molecular simulation (FHAIMS) packages. All the long alkyl side chains in the molecules were replaced by methyl groups to simplify calculation process. We first optimized the geometries of molecules to find optimal molecular structures. We then attached single Au atoms to the S anchors at the two sides of the molecules. After optimizing the geometry, two Au pyramid cluster with 60 atoms were attached to the S anchors, replacing the Au atoms used for geometry optimization. The Landauer transmission across these junctions are finally calculated using the nonequilibrium Green’s function (NEGF) formalism. The Au–S binding energies are calculated with gold pyramid clusters containing 2–7 layers of Au atoms.

Data availability

The main data supporting the findings of this study can be found in the manuscript and the Supplementary information file. Extra data are available from the corresponding authors (Y.Z. and G.Z.) upon request.

Code availability

The data that support the findings was acquired using a custom instrument controlled by custom software (Igor Pro, Wavemetrics). The software is available from <https://www.wavemetrics.com/>.

Received: 26 May 2021; Accepted: 2 March 2022;

Published online: 04 April 2022

References

- Su, T. A., Neupane, M., Steigerwald, M. L., Venkataraman, L. & Nuckolls, C. Chemical principles of single-molecule electronics. *Nat. Rev. Mater.* **1**, 16002 (2016).
- Zang, Y. et al. Electronically transparent Au–N bonds for molecular junctions. *J. Am. Chem. Soc.* **139**, 14845–14848 (2017).
- Ferri, N. et al. Hemilabile ligands as mechanosensitive electrode contacts for molecular electronics. *Angew. Chem. Int. Ed.* **58**, 16583–16589 (2019).
- Xin, N. et al. Concepts in the design and engineering of single-molecule electronic devices. *Nat. Rev. Phys.* **1**, 211–230 (2019).
- Jia, C. et al. Covalently bonded single-molecule junctions with stable and reversible photoswitched conductivity. *Science* **352**, 1443–1445 (2016).
- Zeng, B. F. et al. Selective fabrication of single-molecule junctions by interface engineering. *Small* **16**, e2004720 (2020).
- Leary, E. et al. Incorporating single molecules into electrical circuits. The role of the chemical anchoring group. *Chem. Soc. Rev.* **44**, 920–942 (2015).
- Venkataraman, L., Klare, J. E., Nuckolls, C., Hybertsen, M. S. & Steigerwald, M. L. Dependence of single-molecule junction conductance on molecular conformation. *Nature* **442**, 904–907 (2006).
- Chen, F., Li, X., Hihath, J., Huang, Z. & Tao, N. J. Effect of anchoring groups on single-molecule. *J. Am. Chem. Soc.* **128**, 15874–15881 (2006).
- Park, Y. S. et al. Frustrated rotations in single-molecule junctions. *J. Am. Chem. Soc.* **131**, 10820–10821 (2009).
- Hong, W. et al. Single molecular conductance of tolanes: experimental and theoretical study on the junction evolution dependent on the anchoring group. *J. Am. Chem. Soc.* **134**, 2292–2304 (2012).
- Tour, J. M. et al. Self-assembled monolayers and multilayers of conjugated thiols, -dithiols, and thioacetyl-containing adsorbates. Understanding attachments between potential molecular wires and gold surfaces. *J. Am. Chem. Soc.* **117**, 9529–9534 (1995).
- Olavarria-Contreras, I. J. et al. C–Au covalently bonded molecular junctions using nonprotected alkynyl anchoring groups. *J. Am. Chem. Soc.* **138**, 8465–8469 (2016).
- Tan, L. et al. New tetrathiafulvalene fused-naphthalene diimides for solution-processible and air-stable p-type and ambipolar organic semiconductors. *Chem. Sci.* **3**, 2530 (2012).
- Martin, N. Tetrathiafulvalene: the advent of organic metals. *Chem. Commun.* **49**, 7025–7027 (2013).
- Kim, Y. M., Li, X., Kim, K.-W., Kim, S. H. & Moon, H. C. Tetrathiafulvalene: effective organic anodic materials for WO_3 -based electrochromic devices. *RSC Adv.* **9**, 19450–19456 (2019).
- Jana, A. et al. Functionalised tetrathiafulvalene- (TTF-) macrocycles: recent trends in applied supramolecular chemistry. *Chem. Soc. Rev.* **47**, 5614–5645 (2018).

18. Segura, J. L. & Martín, N. New concepts in tetrathiafulvalene chemistry. *Angew. Chem. Int. Ed.* **40**, 1372 (2001).
19. Spruell, J. M. et al. Highly stable tetrathiafulvalene radical dimers in [3]catenanes. *Nat. Chem.* **2**, 870–879 (2010).
20. Asakawa, M. et al. Electrochemically induced molecular motions in pseudorotaxanes: a case of dual-mode (oxidative and reductive) dethreading. *Chem. Eur. J.* **3**, 1992 (1997).
21. Aviram, A. & Ratner, M. A. Molecular rectifiers. *Chem. Phys. Lett.* **19**, 277–283 (1974).
22. Taniguchi, M., Tsutsui, M., Shoji, K., Fujiwara, H. & Kawai, T. Single-molecule junctions with strong molecule-electrode coupling. *J. Am. Chem. Soc.* **131**, 14146 (2009).
23. Kay, N. J. et al. Single-molecule electrochemical gating in ionic liquids. *J. Am. Chem. Soc.* **134**, 16817–16826 (2012).
24. García, R. et al. Single-molecule conductance of a chemically modified, pi-extended tetrathiafulvalene and its charge-transfer complex with F₄TCNQ. *J. Org. Chem.* **11**, 1068–1078 (2015).
25. O'Driscoll, L. J. et al. Electrochemical control of the single molecule conductance of a conjugated bis(pyrrolo)tetrathiafulvalene based molecular switch. *Chem. Sci.* **8**, 6123–6130 (2017).
26. Parker, C. R. et al. A comprehensive study of extended tetrathiafulvalene cruciform molecules for molecular electronics: synthesis and electrical transport measurements. *J. Am. Chem. Soc.* **136**, 16497–16507 (2014).
27. Manso, M. et al. Synthesis and single-molecule conductances of neutral and cationic indenofluorene-extended tetrathiafulvalenes: Kondo effect molecules. *J. Org. Chem.* **81**, 8406–8414 (2016).
28. Wei, Z. et al. Molecular junctions based on SAMs of cruciform oligo(phenylene ethynylene)s. *Langmuir* **28**, 4016–4023 (2012).
29. Chen, G. M. & Gao, C. Y. Bis(1,3-dithiol-2-carbonyl) fused naphthyl imide derivative and synthesis method thereof. CN105461737-A (P) (2016).
30. Xu, B. & Tao, N. Measurement of single-molecule resistance by repeated formation of molecular junctions. *Science* **301**, 1221–1223 (2003).
31. Yin, X. et al. A reversible single-molecule switch based on activated antiaromaticity. *Sci. Adv.* **3**, ea02615 (2017).
32. Li, Y. et al. Three-state single-molecule naphthalenediimide switch: integration of a pendant redox unit for conductance tuning. *Angew. Chem. Int. Ed.* **54**, 13586–13589 (2015).
33. Kamenetska, M. et al. Formation and evolution of single-molecule junctions. *Phys. Rev. Lett.* **102**, 126803 (2009).
34. Wartelle, C. et al. First signals of electrochemically oxidized species of TTF and TTM-TTF: A study by in situ spectroelectrochemical FTIR and DFT calculations. *Phys. Chem. Chem. Phys.* **5**, 4672–4679 (2003).
35. Hofmann, O. T., Rangger, G. M. & Zojer, E. Reducing the metal work function beyond Pauli pushback: a computational investigation tetrathiafulvalene and viologen on coinage metal surfaces. *J. Phys. Chem. C.* **112**, 20357–20365 (2008).
36. Fernandez-Torrente, I. et al. Long-range repulsive interaction between molecules on a metal surface induced by D-A-D transfer. *Phys. Rev. Lett.* **99**, 176103 (2007).
37. Jethwa, S. J. et al. Adsorption of a dihydro-TTF derivative on Au(111) via a thiolate complex bonding to gold adatoms. *Chem. Commun.* **50**, 10140–10143 (2014).
38. Heimel, G. et al. Charged and metallic molecular monolayers through surface-induced aromatic stabilization. *Nat. Chem.* **5**, 187–194 (2013).
39. Stanger, A. Aromatic stabilization energy and magnetic properties in fulvalenes: is there a connection between these two aromaticity indices? *J. Org. Chem.* **78**, 12374–12380 (2013).
40. Blum, V. et al. Ab initio molecular simulations with numeric atom-centered orbitals. *Comput. Phys. Commun.* **180**, 2175–2196 (2009).
41. Havu, V., Blum, V., Havu, P. & Scheffler, M. Efficient integration for all-electron electronic structure calculation using numeric basis functions. *J. Comput. Phys.* **228**, 8367–8379 (2009).
42. Perdew, J. P., Burke, K. & Ernzerhof, M. Generalized gradient approximation made simple. *Phys. Rev. Lett.* **77**, 3865–3868 (1996).
43. Vladyka, A. et al. In-situ formation of one-dimensional coordination polymers in molecular junctions. *Nat. Commun.* **10**, 262 (2019).
44. Inkpen, M. S. et al. Non-chemisorbed gold-sulfur binding prevails in self-assembled monolayers. *Nat. Chem.* **11**, 351–358 (2019).
45. Quinn, J. R. et al. Single-molecule junction conductance through diaminoacenes. *J. Am. Chem. Soc.* **129**, 6714–6715 (2007).
46. Meisner, J. S. et al. Importance of direct metal-pi coupling in electronic transport through conjugated single-molecule junctions. *J. Am. Chem. Soc.* **134**, 20440–20445 (2012).
47. Capozzi, B. et al. Length-dependent conductance of oligothiophenes. *J. Am. Chem. Soc.* **136**, 10486–10492 (2014).
48. Valkenier, H. et al. Cross-conjugation and quantum interference: a general correlation? *Phys. Chem. Chem. Phys.* **16**, 653–662 (2014).
49. Dell, E. J., Capozzi, B., Xia, J., Venkataraman, L. & Campos, L. M. Molecular length dictates the nature of charge carriers in single-molecule junctions of oxidized oligothiophenes. *Nat. Chem.* **7**, 209–214 (2015).
50. Zang, Y. et al. Resonant transport in single diketopyrrolopyrrole junctions. *J. Am. Chem. Soc.* **140**, 13167–13170 (2018).
51. Tang, Y. et al. Electric field-induced assembly in single-stacking terphenyl junctions. *J. Am. Chem. Soc.* **142**, 19101–19109 (2020).
52. Li, Z. & Borguet, E. Determining charge transport pathways through single porphyrin molecules using scanning tunneling microscopy break junctions. *J. Am. Chem. Soc.* **134**, 63–66 (2012).
53. Liu, Z. F. et al. Control of single-molecule junction conductance of porphyrins via a transition-metal center. *Nano Lett.* **14**, 5365–5370 (2014).
54. Park, Y. S. et al. Contact chemistry and single-molecule conductance: a comparison of phosphines, methyl sulfides, and amines. *J. Am. Chem. Soc.* **129**, 15768–15769 (2007).
55. Li, J. et al. Mechanical single-molecule potentiometers with large switching factors from ortho-pentaphenylene foldamers. *Nat. Commun.* **12**, 167 (2021).
56. Meisner, J. S. et al. A single-molecule potentiometer. *Nano Lett.* **11**, 1575–1579 (2011).
57. Ismael, A. K. et al. Side-group-mediated mechanical conductance switching in Molecular Junctions. *Angew. Chem. Int. Ed.* **129**, 15580–15584 (2017).

Acknowledgements

We acknowledge financial support from the National Natural Science Foundation of China (22073109, 21871271, 21933012, and 21833005), Chinese Academy of Sciences (GJTD-2020-02, XDPB13), and the CAS-Croucher Funding Scheme for Joint Laboratories.

Author contributions

Y.Z., G.Z., and D. Zhang conceived the idea and designed the experiments. Q.Z. synthesized and characterized the molecules. K.S., X.S., and Y.Z. carried out the STM-BJ measurements and analyzed the data. K.S., J.L., and Y.Z. performed DFT calculations. D. Zhu commented on the data. The manuscript was written by Y.Z. and K.S. with contributions from all other authors.

Competing interests

The authors declare no competing interests.

Additional information

Supplementary information The online version contains supplementary material available at <https://doi.org/10.1038/s41467-022-29483-2>.

Correspondence and requests for materials should be addressed to Guanxin Zhang or Yaping Zang.

Peer review information *Nature Communications* thanks the anonymous reviewer(s) for their contribution to the peer review of this work.

Reprints and permission information is available at <http://www.nature.com/reprints>

Publisher's note Springer Nature remains neutral with regard to jurisdictional claims in published maps and institutional affiliations.



Open Access This article is licensed under a Creative Commons Attribution 4.0 International License, which permits use, sharing, adaptation, distribution and reproduction in any medium or format, as long as you give appropriate credit to the original author(s) and the source, provide a link to the Creative Commons license, and indicate if changes were made. The images or other third party material in this article are included in the article's Creative Commons license, unless indicated otherwise in a credit line to the material. If material is not included in the article's Creative Commons license and your intended use is not permitted by statutory regulation or exceeds the permitted use, you will need to obtain permission directly from the copyright holder. To view a copy of this license, visit <http://creativecommons.org/licenses/by/4.0/>.

© The Author(s) 2022